Soft Matter

Accepted Manuscript

This article can be cited before page numbers have been issued, to do this please use: C. A. Feigeles, A. Brasovs, A. Puchalski, O. Laukat, K. Kornev and K. L. Weirich, *Soft Matter*, 2025, DOI: 10.1039/D5SM00508F.

ROYAL SOCIETY OF CHEMISTRY

rsc.li/soft-matter-journal

View Article Online
DOI: 10.1039/D5SM00508F

Protein condensates induce biopolymer filament bundling and network remodeling via capillary interactions

Carolyn A. Feigeles[a], Artis Brasovs[a], Adam Puchalski[a], Olivia Laukat[a], Konstantin G. Kornev[a], and Kimberly L. Weirich[a*]

[a]Department of Materials Science & Engineering, Clemson University, Clemson, SC 29634

*corresponding author: weirich@clemson.edu

View Article Online
DOI: 10.1039/D5SM00508F

Abstract
Many cellular processes are regulated by biopolymers that are self-assembled into higher order structures by protein interactions. The actin cytoskeleton, which forms the mechanical structure of cells, consists of actin filaments that are assembled into networks and bundles by protein cross-linkers. Specific network and bundle microstructures are determined by the type of cross-linker and support different physiological functions. Recently, there is also evidence that protein condensates can nucleate bundle formation with cytoskeletal filaments. Here, we find that protein condensates interact with pre-polymerized actin filaments to form networks of bundles. The condensates absorb on actin bundles and relax into barrel shaped droplets, evocative of drops of simple liquids on fibers. We investigate the condensate spreading and measure contact angle that condensates make with bundles. Intriguingly, condensates at the intersection of bundles cause capillary bridges which induce network remodeling. Our results suggest that network formation, bundling, and remodeling in biopolymer assemblies could be induced by capillary interactions due to condensates.

Introduction
An important class of biological materials are the dynamic protein assemblies in cells comprising the cytoskeleton which regulate mechanical processes. These vastly different physiological processes, such as such as extending protrusions and controlling shape, exerting forces, and cargo transport are mediated by a discrete set of cytoskeletal proteins that organize filaments into assemblies with different mechanical properties derived from specific microstructures (1–4). The cytoskeletal protein, actin, forms filaments which arrange into networks, bundles, and networks of bundles. It is well known that protein cross-linkers, which have two or more domains that bind to actin, arrange actin into the various assemblies, where the microstructure derives from the cross-linker properties.

Liquid-liquid phase separated condensates have emerged as another class of cellular assemblies (5–7). The liquid behavior of protein condensates suggests that condensates have interactions with various cellular surfaces, such as wetting of membranes and filaments, that potentially could induce mechanical deformations or higher-order structure formation via capillary-like interactions (8–10). For example, it is known that when a liquid drop interacts with a fiber, in the limit that the fiber bending energy is small compared to the interfacial energy, the fiber bends, wrapping around the drop at the interface or engulfed within the drop (11). In the limit where the bending energy is large compared to the interfacial energy, the drop beads or spreads on the fiber. When multiple wettable fibers interact with the same drop, the fibers are drawn together via capillary bridges (12). The capillary bridges have the potential to induce the formation of fiber aggregates and higher order structures (13). Despite extensive research on drops interacting with fibers that have a cross-section much greater than the scale of the liquid molecules (14–16), little is known about how drops interact with materials that have length scale on the order of the liquid molecules, such as the role of wetting and capillary interactions in assembly formation of protein condensates and protein filaments.

Here, we investigate the interaction of protein condensates with actin filaments. We find that actin filaments and condensates colocalize into bundles that bridge together into a space spanning network. By observing the interaction of a single condensate and a bundle of actin filaments, we find direct evidence that condensates spread along a bundle evocative of macroscopic systems of liquid drops on fibers. We fit the condensate shape to a model of an unduloidal drop to measure the contact angle and capillary pressure of condensates on actin bundles (14). We find that condensates can bridge filaments and condensates on separate bundles can coalesce, inducing network formation and remodeling. Together, these results indicate a capillary-based mechanism for cytoskeletal assembly formation, distinct from cross-linker induced bundling.

View Article Online
DOI: 10.1039/D5SM00508F

Results

Condensates and filaments colocalize in bundles

To create actin networks, we polymerize actin filaments by adding 2.64 μM actin monomer to actin polymerization buffer in the presence of a depletion agent, which causes filaments to accumulate at the surfaces of the sample chamber (Fig. 1A and 1B) (17). We add 4 μM FUS protein to the pre-polymerized actin. At this concentration, which is similar to physiological concentrations of FUS in the nucleus (18), FUS without actin forms protein condensates in buffer conditions (Fig. 1C), consistent with liquid-liquid phase-separated condensates reported previously for similar conditions (19). Upon adding FUS condensates to the actin network, actin filaments rapidly begin to bundle (Fig. 1D and Movie S1). First, small segments of condensate ((Fig. 1D, left column (gray) and right column (blue)); Fig. S1 (column 1)) accumulate between actin filaments (Fig. 1D, green; Fig. S1 (column 2)), inducing bundling (0-40 s). Eventually, the condensates cover the length of the bundles (>200 s). Inspecting the intensity along a line perpendicular to the bundle length reveals that condensates and actin have maxima at the same location (Fig. 1E). This indicates that actin filaments and condensates are colocalized in bundles with an average bundle thickness is 0.23 ± 0.10 μm. This is comparable to the average thickness of actin bundles formed by physiological cross-linkers (20, 21). Additionally, the bundles appear stiffer than single filaments. To quantify this, we take the ratio of the contour length, L_c, to the end-to-end length, *l*. This ratio shows that the condensate-induced actin bundles are straight on length scale upwards of 40 μm (Fig. S2), compared to the persistence length of a single actin filament, which is approximately 10 μm (22).

Condensates adsorb on bundles and form drops

When an individual condensate in solution approaches actin filaments previously bundled by condensate, the condensate spreads on the bundle (Fig. 2A and Movie S2). The free condensate is initially spherical before it absorbs to the bundle (Fig. 2A, 0-15 s), and changes morphology as it spreads into a final, barrel-shape (15-60 s). To characterize the condensate spreading, we measure the aspect ratio, $\frac{2R_{max}}{l}$, of the condensate over time, where R_{max} and l are defined in Fig. 2B. The aspect ratio is initially ~1 prior to the condensate adsorbing onto the actin bundle, consistent with a spherical droplet. As the condensate spreads on the bundle, the aspect ratio decreases to ~0.7, with a characteristic decay time of ~5.8 s from an exponential fit (Fig. 2B). The condensate remains barrel-shaped on the bundle until the end of observation (~200 s), suggesting that the bundle cannot accommodate more condensate incorporation during this spreading event. We find the spreading dynamics follows a similar trend for different condensate sizes (Fig. S3).

We measure the contact angle between the condensate and filaments bundled by condensates, which provides information regarding relative surface energies of components (23, 24). To measure the contact angle (Fig. 2C, inset; for more detail see Fig. 5), we first extract the condensate contour and fit to an unduloid (Fig. 5). Across 28 condensates, the contact angle is scattered without dependence on condensate radius (Fig. S4). Normalizing the condensate radius, R_{max}, by the fiber radius, R_f, (Fig. S5) reveals that the contact angle remains constant across a range of condensate sizes with respect to bundle radius (Fig. 2C, n=28). The low average contact angle, θ = 39.5° ± 9.01°, indicates in these buffer conditions, that it is favorable for FUS to wet bundles (Fig. 2A, (25)). A contact angle closer to zero might have been expected, in the limit where condensates completely coat the bundle, since the condensates are spreading on bundles that condensates have already wet (Fig. 2E i). The deviation of the contact angle between the condensate and bundle from zero suggests that some parts of the actin within the bundle are directly exposed to the buffer.

View Article Online
DOI: 10.1039/D5SM00508F

To distinguish between cases where the condensates are completely or partially coating the bundle (Fig. 2E), we consider the capillary pressure which is the pressure between two immiscible fluids at an interface (8, 15, 26). The capillary pressure, $\Delta P_{condensate}$, between the condensate and bundle for an unduloid drop is $\Delta P_{condensate} = 2\gamma\frac{R_{max}-R_f cos\theta}{R_{max}^2-R_f^2}$, where γ is the interfacial tension of condensates (14). Assuming an interfacial tension for FUS condensates of 90 μNm^{-1} (27), which has an order of magnitude consistent with measurements in our system (Fig. S6), we found that the capillary pressure ranges from ~20 to 70 Nm^{-2} (Fig. S7). In the case where the condensate completely wets the bundle, $\Delta P_{condensate}$, would be expected to be equal to the capillary pressure of cylindrical FUS column, $\Delta P_{column} = \frac{\gamma}{R_f}$. We find that the pressure range in the condensate is smaller than the pressure range associated with a FUS column, ~65 to 260 Nm^{-2}. Plotting the dimensionless capillary pressure, $\frac{\Delta P_{condensate} * R_f}{\gamma} = 2\frac{R_f(R_{max}-R_f cos\theta)}{R_{max}^2-R_f^2}$, which is the capillary pressure normalized by the capillary pressure of the cylindrical FUS column, against the condensate radius rescaled by the bundle radius, $\frac{R_{max}}{R_f}$, reveals that for the majority of the tested droplets, this ratio is less than 1 (Fig. 2D), indicating that the completely wet case shown in Fig. 2E (*i)* is inconsistent with the data. In contrast, previous studies of wetting phenomena on fiber systems made of wettable nanofibers showed complete drop absorption (28–31).

To better understand how a barrel-shaped condensate with a positive capillary pressure could be in equilibrium with a bundle of wettable nanofibers that is not completely covered by the fluid column, we consider another scenario of FUS absorption where each condensate meniscus bridging two actin filaments makes an arc of radius R_{FUS} (Fig. 2E *ii* and *iii*). This radius satisfies the equilibrium condition $2\gamma\frac{R_{max}-R_f cos\theta}{R_{max}^2-R_f^2} = \frac{\gamma}{R_{FUS}}$. The data $\frac{R_{max}}{R_f}$ in Fig. 2C, indicates that R_{FUS} ranges between $2.3\,R_f < R_{FUS} < 5.4\,R_f$, suggesting that menisci in the surface grooves of the bundle could have a greater radius of curvature while in equilibrium with the droplet. To evaluate the contact angle, $\theta_{filament}$, that FUS makes with individual actin filaments using the Cassie-Baxter theory (14, 30, 32) one needs to know the filament density in the bundle, which is not available with the current data.

Condensates coalesce on bundles

In addition to condensates adsorbing on bundles and spreading, condensates also come in contact with another condensate that has previously spread on an actin bundle (Fig. 3A and Movie S3). When a spherical condensate approaches a barrel-shaped condensate on a bundle, both condensates quickly (<5 s) merge and transiently form an asymmetric condensate on the bundle (40-45 s). The condensate then redistributes, becoming more symmetric about the bundle as it spreads, finally adopting a barrel shape similar to the adsorbed condensate before coalescence (50 s).

Another case is when two condensates, which have separately adsorbed and spread on a bundle, coalesce. In Figure 3B (Movie S4), a bundle initially (0 s) has a condensate that has already spread and relaxed into a barrel shape (t<0 s; same data as Fig. 2A). When a second larger condensate comes into the focal plane and adsorbs onto the bundle a few microns away from the first (Fig. 3B, 40-120 s), we see it spread. Despite the smaller condensate having a greater capillary pressure than the larger condensate, it does not incorporate into the bundle suggesting that the bundle is fully saturated with the FUS condensate. As the larger condensate spreads, the smaller condensate merges and relaxes into a single barrel-shaped condensate with the sum of the volumes (Fig. 3B, 160 s). We measure the condensate length along the major axis as the two

View Article Online
DOI: 10.1039/D5SM00508F

condensates coalesce. The condensate length shortening is consistent with exponential decay that has relaxation time, τ=14.4 s (Fig. 3C). These data indicate condensates are able to coalesce on bundles similarly to how condensates coalesce with each other in solution. The condensate on the bundle maintains properties of a liquid, as would be expected of a drop of a simple liquid on a fiber.

Condensates bundle filaments

Condensates not only absorb on isolated bundles, but can also exist at the intersection of multiple actin filaments or bundles. In Figure 4A, (Movie S5) condensates at the intersection of bundles (0 min), spread on individual bundles and begin to merge (3-6 min). As they coalesce (Fig. 4A, 9-13 min), the actin bundles and filaments are bridged by the condensate and drawn closer together, until they merge into a larger bundle. This indicates that capillary bridges induce bundling in and remodeling of networks of actin filaments bundled by condensates (Fig. 4B).

The capillarity-induced bundling observed in networks provides insight into mechanism of initial actin filament bundling by condensates. We have not captured condensates interacting with single actin filaments, due to the quick formation of initial bundles. However, we do have evidence that condensates can accumulate in the initial stages of actin bundles in small regions (Fig. 4C, a zoomed in region of data in Fig. 1D), reminiscent of capillary bridge segments formed by droplets between two fibers (12). On the order of tens of seconds, these segments become longer while condensates continue to accumulate in the bundles. A maximal intensity projection of the first 60 s, indicates that the overall network structure is stable during initial bundle formation (Fig. 4D, 0-60 s, compare with Fig. 4C, 0-40 s). However, after condensates have spread throughout actin bundles, the bundles begin merging with neighboring bundles and the network coarsens (Fig. 4C, > 200 s). A maximal intensity projection of data from 60-290 s shows bundle mobility and large changes in network structure (Fig. 4D, 60-290 s).

Discussion

Cytoskeletal assemblies enable a variety of critical physiological functions, supported through variations in microstructures, which have mechanical properties that derive from structure. In cytoskeletal assemblies, the microstructure is predominately known to be regulated through proteins which cross-link cytoskeletal filaments, such as actin and microtubules. In this paper, our results provide direct experimental evidence highlighting the importance of capillary interactions in actin assembly formation via protein condensates. We find that condensates induce actin bundling and network formation, which remodel through capillary bridges and condensate coalescence.

Actin bundling and assembly formation has also been reported in other condensate-filament systems. For example, there are reports of bundles that nucleate out of condensates and cause protrusions, such as actin bundled networks in abLIM1 condensates and aster shaped actin bundles which nucleate from VASP condensates (33, 34). Filaments have also been shown to induce condensate deformation, such as bundles of FUS condensates and actin filaments, where short (~100 nm) actin filaments were found to impart an elasticity that influenced the condensate shape (35). Filaments have also been shown to form bundled rings inside condensates, such as actin in VASP condensates, similar to reports of actin in polyelectrolyte coacervates (19, 33, 36).

In contrast to the experiments which demonstrate assembly formation and colocalization of cytoskeletal filaments and condensates, our evidence directly demonstrates that capillary bridging and condensate coalescence are physical mechanisms of actin network remodeling. The capillary bridging mechanism is consistent with reports of “zippering” bundles (19). Interestingly, the remodeling and responsiveness of cross-linked actin networks derive from cross-linkers ability to

View Article Online
DOI: 10.1039/D5SM00508F

dynamically bind and unbind (37). Capillarity- induced bundling and network remodeling may yield networks with not only different microstructure, but dynamics and properties than cross-linked assemblies. For example, it has recently been reported that vimentin-Y117L condensates in cells stabilize actin stress fibers, reducing actin filament depolymerization in the presence of cytochalasin B (38).

These initial studies are with one type of protein condensate (FUS) interacting with the cytoskeletal filament actin. However, there are many types of protein condensates and cytoskeletal filaments, with different chemistries and structures (19, 38, 39). Ion species and valency is known to be important in both cytoskeletal filament polymerization and interaction with other proteins, as well as for FUS condensate phase separation (40–42). Future research might explore the molecular mechanisms of FUS protein interactions with actin, as well as other protein condensates and the role of ion species and ionic strength, to gain insight into the absorption and spreading process. It would also be interesting to understand if polymer complex coacervates, which can exhibit liquid behavior and are of interest in drug delivery applications, might also influence cytoskeletal filament assembly (36, 43–45).

The capillary induced remodeling of bundled networks directly indicates that actin filaments can be bundled by condensates via capillary interactions, similar to drops that bridge and draw together fibers (12). These bundles potentially have similar microstructures to elongated bundles of filaments that have been reported to nucleate within protein condensates, such as microtubules with tau condensates, and actin with and VASP and abLIM1 condensates (46, 19, 33, 34). Cytoskeletal bundle microstructure is canonically known to be regulated through proteins which cross-link cytoskeletal filaments together, and control mechanics through spacing and cross-linker binding dynamics. Future experiments will investigate how filament packing and bundle mechanics in bundles formed via capillary interactions compares with bundles formed by cross-linking.

We find that condensates absorb and spread on actin filaments, forming barrel-shaped condensates. Notably, the shape is similar to that characteristic of liquid drops collecting on macroscopic fibers, despite the different length scale of actin filaments (diameter is ~7 nm) and molecular details of protein-based liquids (14, 15). In this work, we have focused on condensates spreading along actin filaments that have already been bundled by condensates. For the purposes of this study, we have treated the bundle as a uniform cylinder with a radius of the bundle. On planar surfaces, it is known that the texture and microstructural details of the surface influence drop wetting and spreading (47–50). In our system, the bundle is made of filaments that are packed together with condensate creating a surface that is complex and could be porous without any control of the interfilament spacing. Future research will investigate condensate spreading on bundles with different interfilament spacing, expanding our understanding of how drops spread on porous fibers.

Methods

Protein Preparation

Monomeric actin protein is hydrated from lyophilized powder (>99% pure rabbit skeletal muscle, Cytoskeleton) to 10 mg/mL by adding milliQ water and pipette mixing every five minutes while the solution incubates on ice for 15 minutes. Then, the actin solution is dialyzed against the actin storage buffer (2 mM Tris, 0.1 mM $CaCl_2$, 0.5 mM DTT, 0.2 mM ATP, 1 mM NaN_3, pH 8) for at least three hours on ice. The solution is further dialyzed overnight at 4℃ before flash freezing in liquid nitrogen before storage until use.

Fluorescently labeled actin is prepared by purifying actin from rabbit skeletal muscle acetone

View Article Online
DOI: 10.1039/D5SM00508F

powder (Pel-Freez Biologicals) using a protocol adapted from (51). The actin was labeled with tetramethylrhodamine-6-maleimide (TMR) and stored in actin storage buffer. FUS GFP purified from insect cells (50 mM Tris-HCl, 500 mM KCl, 1 mM DTT, pH 7.4) was received as a gift from the A. Hyman lab (18, 35).

Concentration of protein stocks are determined through absorbance measurements using an extinction coefficient for actin of 42680 $M^{-1}cm^{-1}$ at 280 nm. The final protein solutions are aliquoted and then flash-frozen in liquid nitrogen and stored at -80℃. Actin is used within three days of thawing, and FUS is used within one day of thawing. After thawing, the proteins are kept at 4℃ until use.

Microscope Sample

The sample chamber consists of a borosilicate cylinder (Corning) epoxied to the center of a borosilicate coverslip (Fisherbrand). Prior to assembling, the glass is rinsed twice with ethanol and water before drying with filtered air. To passivate the coverslip surface, 2 wt% 008-Fluorosurfactant in HFE7500 oil (RAN Biotechnologies) is added to the sample chamber and excess surfactant solution is removed via pipette immediately prior to adding the sample.

To polymerize the actin filaments, actin monomer is added to a buffer solution (2 mM Tris-HCl, 2 mM $MgCl_2$, 0.50 wt% β-mercaptoethanol, 0.3 mM ATP, and 0.40 wt% methylcellulose) such that the concentration in the final sample (after adding FUS) is 2.64 μM actin monomer (0.264 μM labeled with TMR). The actin is then incubated for at least 20 minutes before introducing it to the sample chamber. Finally, FUS is added to the sample, such that the final FUS concentration is between 2.64 to 5.28 μM, depending on the particular sample in a final buffer of 4 mM Tris-HCl, 2 mM $MgCl_2$, 0.50 wt% β-mercaptoethanol, 0.3 mM ATP, 0.40 wt% methylcellulose, 0.625 wt% glycerol, 20 mM KCl, and 0.04 mM DTT). The sample is gently pipette mixed.

Microscopy

Samples are imaged using a Nikon Eclipse TI2 microscope equipped with a W1 spinning disk confocal head (Yokogawa) with an ORCA-Fusion CMOS camera (Hamamatsu) using a 60×, 1.49 numerical aperture Apo TIRF objective (Nikon). The samples are illuminated using 488 nm and 561 nm laser lines.

Image Analysis

To determine whether actin and FUS condensates are colocalized in a bundle, we measured the fluorescence intensity associated with each protein along a line that is perpendicular to the long axis of the bundle. To quantify the aspect ratio of condensates, we use ImageJ to measure the lengths of the major axis and perpendicular minor axis of the condensate (52). The aspect ratio is the major axis to minor axis. To visualize bundle motion during network coarsening, we used the maximum intensity projection function of ImageJ to compress intensity information from a stack of images into a single image.

Bundle radius measurement

To determine the bundle radius, we first used the plot profile function of ImageJ to measure the intensity along a line that is perpendicular to the bundle length and extends at least 20 pixels beyond the bundle on either side. This information was then plotted and fit to a Gaussian using the following functional form

$$I_0 + \frac{I_B}{\sigma\sqrt{2\pi}} e^{-\left(\frac{(x-x_0)^2}{2\sigma^2}\right)} \quad (1)$$

View Article Online
DOI: 10.1039/D5SM00508F

where I_0 is the intensity of the background, I_B is the intensity associated with the bundle, σ is the standard deviation of the intensity distribution, and x_0 is the location of the maximum intensity. We define the radius of the bundle to be the full width half max of the Gaussian, $2\sigma\sqrt{2ln2}$. Gaussian fits had an average R^2 = 0.992, with a minimum of R^2= 0.967. For each single bundle, the radius was measured at 3 points. The reported radius is an average of 30 bundles.

Contact angle and shape analysis

The contact angle with the substrate was measured for FUS wrapping around the fiber- like bundle. The formation of a static axisymmetric meniscus with barrel-shaped morphology (Fig. 5) was used as an indication for reaching an equilibrium condition. We modified the Carroll method (53) designed for the characterization of monofilaments, where the droplet length could be accurately measured. However, the contact lines are hardly detectable on a fiber bundle. As the contact angle is sensitive to this metric, so the Carroll method has been modified using the modern image processing tools to use the drop profile rather than Carroll's integral characteristics (14). The droplet shape profile was extracted using MATLAB image processing and edge detection algorithms. The contour was split in four sections – along the long axis at the middle of the fiber, and perpendicular to the fiber at the widest part of the barrel-shaped meniscus (Fig. 5). Contour data was separated from the fiber contour at the contact line, and the droplet profile was fit with the unduloidal function (Eq. 3) based on Young-Laplace equation (Eq. 2):

$$\frac{\Delta p}{\sigma} = \frac{d\gamma}{dy}\cos(\gamma) + \frac{\sin(\gamma)}{\gamma} \tag{2}$$

$$\frac{dy}{dx} = \sqrt{1 - [\frac{\Delta p}{2\sigma}y - \frac{c}{y}]^2}/(\frac{\Delta p}{2\sigma}y - \frac{c}{y})^2 = \sqrt{\frac{1}{\frac{\Delta p}{2\sigma}y - \frac{c}{y}} - 1} \tag{3}$$

where Δp is the pressure difference between inside and outside of the droplet, σ is the interfacial tension, γ is the angle that the normal vector to the droplet surface creates with the fiber long axis, c is the fitting constant, and $r_1 = \frac{ds}{dy}$, $r_2 = \frac{\gamma}{\sin(\gamma)}$ are the principal radii of curvature of the liquid interface. The MATLAB function ode45 was used to find the best fit using the least square method with initial condition at the contact line with the bundle $y_0 = R_f$ and $x_0 = 0$. The fitting parameters $\frac{\Delta p}{2\sigma}$ and c were defined through measurable parameters as (14):

$$c = R_f^2 \cdot \frac{R_b \sin(\theta_b) - \frac{R_b^2 \cos(\theta)}{R_f}}{R_b^2 - R_f^2} \tag{4}$$

$$\frac{\Delta p}{2\sigma} = \frac{\cos(\theta)}{R_f} + \frac{c}{R_f^2} \tag{5}$$

where R_f is the radius of the bundle, R_b is the radius of the barrel-shaped droplet at the cut-off, θ is the receding contact angle, θ_b is the angle of the contour against the y axis at the cut-off as shown in Fig. 5. Once parameter $\frac{\Delta p}{2\sigma}$ is found, the contact angle is obtained by solving Eq.(5) for θ. As illustrated in Fig. 5 B, the FUS droplet profile fully follows the unduloidal shape.

Acknowledgements

We thank Avinash Patel and Tony Hyman for the gift of FUS-GFP. This research was supported in part by Clemson University's Creative Inquiry + Undergraduate Research Program.

References

1. L. Blanchoin, R. Boujemaa-Paterski, C. Sykes, J. Plastino, Actin Dynamics, Architecture,

View Article Online
DOI: 10.1039/D5SM00508F

and Mechanics in Cell Motility. *Physiological Reviews* **94**, 235–263 (2014).

2. O. Lieleg, M. M. A. E. Claessens, A. R. Bausch, Structure and dynamics of cross-linked actin networks. *Soft Matter* **6**, 218–225 (2010).

3. S. Banerjee, M. L. Gardel, U. S. Schwarz, The Actin Cytoskeleton as an Active Adaptive Material. *Annu. Rev. Condens. Matter Phys.* **11**, 421–439 (2020).

4. T. D. Pollard, J. A. Cooper, Actin, a Central Player in Cell Shape and Movement. *Science* **326**, 1208–1212 (2009).

5. C. P. Brangwynne, *et al.*, Germline P Granules Are Liquid Droplets That Localize by Controlled Dissolution/Condensation. *Science* **324**, 1729–1732 (2009).

6. S. F. Banani, H. O. Lee, A. A. Hyman, M. K. Rosen, Biomolecular condensates: organizers of cellular biochemistry. *Nat Rev Mol Cell Biol* **18**, 285–298 (2017).

7. S. Alberti, A. A. Hyman, Biomolecular condensates at the nexus of cellular stress, protein aggregation disease and ageing. *Nat Rev Mol Cell Biol* **22**, 196–213 (2021).

8. B. Gouveia, *et al.*, Capillary forces generated by biomolecular condensates. *Nature* **609**, 255–264 (2022).

9. A. Mangiarotti, R. Dimova, Biomolecular Condensates in Contact with Membranes. *Annual Review of Biophysics* **53**, 319–341 (2024).

10. T. Wiegand, A. A. Hyman, Drops and fibers — how biomolecular condensates and cytoskeletal filaments influence each other. *Emerging Topics in Life Sciences* **4**, 247–261 (2020).

11. R. D. Schulman, *et al.*, Elastocapillary bending of microfibers around liquid droplets. *Soft Matter* **13**, 720–724 (2017).

12. C. Duprat, S. Protière, A. Y. Beebe, H. A. Stone, Wetting of flexible fibre arrays. *Nature* **482**, 510–513 (2012).

13. P. Wang, R. Bian, Q. Meng, H. Liu, L. Jiang, Bioinspired Dynamic Wetting on Multiple Fibers. *Advanced Materials* **29**, 1703042 (2017).

14. Y. Sun, A. V. Bazilevsky, K. G. Kornev, Classification of axisymmetric shapes of droplets on fibers. Could non-wettable fibers support axisymmetric droplets? *Physics of Fluids* **35**, 072004 (2023).

15. A. Gupta, *et al.*, Effect of gravity on the shape of a droplet on a fiber: Nearly axisymmetric profiles with experimental validation. *Phys. Rev. Fluids* **6**, 063602 (2021).

16. H. B. Eral, *et al.*, Drops on functional fibers: from barrels to clamshells and back. *Soft Matter* **7**, 5138 (2011).

17. S. Stam, *et al.*, Filament rigidity and connectivity tune the deformation modes of active biopolymer networks. *Proc. Natl. Acad. Sci. U.S.A.* **114** (2017).

View Article Online
DOI: 10.1039/D5SM00508F

18. A. Patel, *et al.*, A Liquid-to-Solid Phase Transition of the ALS Protein FUS Accelerated by Disease Mutation. *Cell* **162**, 1066–1077 (2015).

19. K. Graham, *et al.*, Liquid-like VASP condensates drive actin polymerization and dynamic bundling. *Nat. Phys.* **19**, 574–585 (2023).

20. K. L. Weirich, S. Stam, E. Munro, M. L. Gardel, Actin bundle architecture and mechanics regulate myosin II force generation. *Biophysical Journal* **120**, 1957–1970 (2021).

21. D. L. Stokes, D. J. DeRosier, Growth conditions control the size and order of actin bundles in vitro. *Biophysical Journal* **59**, 456–465 (1991).

22. F. Gittes, B. Mickey, J. Nettleton, J. Howard, Flexural rigidity of microtubules and actin filaments measured from thermal fluctuations in shape. *The Journal of cell biology* **120**, 923–934 (1993).

23. D. Y. Kwok, A. W. Neumann, Contact angle measurement and contact angle interpretation. *Advances in Colloid and Interface Science* **81**, 167–249 (1999).

24. A. Marmur, C. Della Volpe, S. Siboni, A. Amirfazli, J. W. Drelich, Contact angles and wettability: towards common and accurate terminology. *Surface Innovations* **5**, 3–8 (2017).

25. D. Seveno, T. D. Blake, J. De Coninck, Young's Equation at the Nanoscale. *Phys. Rev. Lett.* **111**, 096101 (2013).

26. C. D. Willett, M. J. Adams, S. A. Johnson, J. P. K. Seville, Capillary Bridges between Two Spherical Bodies. *Langmuir* **16**, 9396–9405 (2000).

27. M. Ijavi, *et al.*, Surface tensiometry of phase separated protein and polymer droplets by the sessile drop method. *Soft Matter* **17**, 1655–1662 (2021).

28. A. V. Neimark, *et al.*, Hierarchical Pore Structure and Wetting Properties of Single-Wall Carbon Nanotube Fibers. *Nano Lett.* **3**, 419–423 (2003).

29. C.-C. Tsai, *et al.*, Nanoporous artificial proboscis for probing minute amount of liquids. *Nanoscale* **3**, 4685 (2011).

30. C.-C. Tsai, Y. Gu, K. G. Kornev, Wetting of nanofiber yarns. *Colloids and Surfaces A: Physicochemical and Engineering Aspects* **459**, 22–30 (2014).

31. L. Zhang, *et al.*, Wettability of carbon nanotube fibers. *Carbon* **122**, 128–140 (2017).

32. A. B. D. Cassie, S. Baxter, Wettability of porous surfaces. *Trans. Faraday Soc.* **40**, 546 (1944).

33. K. Graham, *et al.*, Liquid-like condensates mediate competition between actin branching and bundling. *Proc. Natl. Acad. Sci. U.S.A.* **121**, e2309152121 (2024).

34. S. Yang, *et al.*, Self-construction of actin networks through phase separation–induced abLIM1 condensates. *Proc. Natl. Acad. Sci. U.S.A.* **119**, e2122420119 (2022).

35. D. R. Scheff, *et al.*, Tuning shape and internal structure of protein droplets *via* biopolymer

View Article Online
DOI: 10.1039/D5SM00508F

filaments. *Soft Matter* **16**, 5659–5668 (2020).

36. P. M. McCall, *et al.*, Partitioning and Enhanced Self-Assembly of Actin in Polypeptide Coacervates. *Biophysical Journal* **114**, 1636–1645 (2018).

37. T. D. Pollard, Actin and Actin-Binding Proteins. *Cold Spring Harb Perspect Biol* **8**, a018226 (2016).

38. A. Basu, *et al.*, Vimentin undergoes liquid–liquid phase separation to form droplets which wet and stabilize actin fibers. *Proc. Natl. Acad. Sci. U.S.A.* **122**, e2418624122 (2025).

39. A. Vidal Ceballos, *et al.*, Liquid to solid transition of elastin condensates. *Proc. Natl. Acad. Sci. U.S.A.* **119**, e2202240119 (2022).

40. J. X. Tang, P. A. Janmey, The Polyelectrolyte Nature of F-actin and the Mechanism of Actin Bundle Formation. *Journal of Biological Chemistry* **271**, 8556–8563 (1996).

41. S. Qamar, *et al.*, FUS Phase Separation Is Modulated by a Molecular Chaperone and Methylation of Arginine Cation-π Interactions. *Cell* **173**, 720-734.e15 (2018).

42. Z. Feng, X. Chen, X. Wu, M. Zhang, Formation of biological condensates via phase separation: Characteristics, analytical methods, and physiological implications. *Journal of Biological Chemistry* **294**, 14823–14835 (2019).

43. A. B. Marciel, E. J. Chung, B. K. Brettmann, L. Leon, Bulk and nanoscale polypeptide based polyelectrolyte complexes. *Advances in Colloid and Interface Science* **239**, 187–198 (2017).

44. A. W. Folkmann, A. Putnam, C. F. Lee, G. Seydoux, Regulation of biomolecular condensates by interfacial protein clusters. *Science* **373**, 1218–1224 (2021).

45. M. J. Harrington, R. Mezzenga, A. Miserez, Fluid protein condensates for bio-inspired applications. *Nat Rev Bioeng* **2**, 260–278 (2023).

46. A. Hernández-Vega, *et al.*, Local Nucleation of Microtubule Bundles through Tubulin Concentration into a Condensed Tau Phase. *Cell Reports* **20**, 2304–2312 (2017).

47. R. N. Wenzel, RESISTANCE OF SOLID SURFACES TO WETTING BY WATER. *Ind. Eng. Chem.* **28**, 988–994 (1936).

48. P. S. Swain, R. Lipowsky, Contact Angles on Heterogeneous Surfaces: A New Look at Cassie's and Wenzel's Laws. *Langmuir* **14**, 6772–6780 (1998).

49. S. M. Kumar, A. P. Deshpande, Dynamics of drop spreading on fibrous porous media. *Colloids and Surfaces A: Physicochemical and Engineering Aspects* **277**, 157–163 (2006).

50. P. Zhu, R. Chen, C. Zhou, Y. Tian, L. Wang, Asymmetric fibers for efficient fog harvesting. *Chemical Engineering Journal* **415**, 128944 (2021).

51. J. A. Spudich, S. Watt, The Regulation of Rabbit Skeletal Muscle Contraction. *Journal of Biological Chemistry* **246**, 4866–4871 (1971).

View Article Online
DOI: 10.1039/D5SM00508F

52. J. Schindelin, *et al.*, Fiji: an open-source platform for biological-image analysis. *Nat Methods* **9**, 676–682 (2012).

53. B. J. Carroll, The accurate measurement of contact angle, phase contact areas, drop volume, and Laplace excess pressure in drop-on-fiber systems. *Journal of Colloid and Interface Science* **57**, 488–495 (1976).

Figure Captions

Figure 1. FUS condensates and actin filaments colocalize in bundles. (A) Schematic of experimental setup. FUS condensates (blue) are added to actin filaments (green) crowded to a passivated surface. (B) Fluorescence microscopy image of entangled actin network (2.64 μM) crowded to a surface. Scale bar is 20 μm. (C) Fluorescence microscopy image of FUS condensates (4 μM). Scale bar is 20 μm. (D) Fluorescence images of FUS condensates (4 μM FUS) and actin network bundling and remodeling over time. Left column images are FUS (grey). Right column is FUS (blue) and actin (green) merged. Scale bar is 10 μm. (E) Distribution of intensity of FUS and actin over a given distance, showing colocalization within the network.

Figure 2. FUS condensates adsorb on actin bundles and form barrel-shaped condensates. (A) Fluorescence microscopy images of a FUS condensate absorbing to and spreading over an actin bundle. The final sample concentration is 2.64 μM actin and 4.4 μM FUS. Scale bar is 5 μm. (B) Aspect ratio ($2R_{max}/l$) of condensate in (A) as a function of time. Images of condensate cropped at the bundle interface over time (top). (C) Schematic of contact angle definition, θ (inset). Contact angle as a function of the condensate radius, $R_{\max}$, rescaled by the actin bundle radius, R_f (n=28 condensates). (D) Dependence of the dimensionless capillary pressure, $2\frac{R_f(R_{max}-R_f cos\theta)}{R_{max}^2-R_f^2}$, on the droplet radius normalized by the fiber radius, $\frac{R_{max}}{R_f}$, calculated for 28 FUS condensates. (E) Cartoon of different potential condensate-filament surfaces in bundles. i) the filaments are bundled inside a column of condensate. ii) filaments and condensates coexist at the surface, forming a surface where filaments can be directly in contact with buffer or condensates form liquid bridges that meet actin filaments at acute contact angles. iii) filaments and condensates coexist at the surface as in (ii), but liquid bridges have larger radius of curvature.

Figure 3. FUS Condensates Coalesce on Filaments and Bundles. (A) Fluorescence microscopy images of a FUS condensate free in solution merging with a barrel-shaped FUS condensate on bundle (2.64 μM actin and 5.28 μM FUS). Scale bar is 2 μm. (B) Fluorescence microscopy images of a FUS condensate spreading on a bundle and merging with a previously absorbed FUS condensate (2.64 μM actin and 4.4 μM FUS). Scale bar is 5 μm. (C) The length of two condensates coalescing on an actin bundle (data in B) as a function of time (black filled circles). Exponential fit (red solid line) has a characteristic decay of τ=14.4 s.

Figure 4. FUS condensates bundle and remodel actin networks via capillary bridges. (A) Fluorescence microscopy images of FUS condensates (blue) at intersection of multiple actin (green) filaments bundled by condensate (0 min). Condensates spread and begin to coalesce (3-6 min), bringing filaments together (9-13 min). Sample concentration is 2.64 μM actin and 2.64 μM FUS. Scale bar is 5 μm. (B) Cartoon of capillary bridging of a condensate (blue) between actin filaments (green). (C) Fluorescence microscopy images of absorbed FUS condensates spreading along and bundling actin filaments. Data is magnified region of data in Figure 1D. Scale bar is 2 μm. (D) Maximum intensity projection of the network shown in Fig. 4B. The initial projection (0-60

View Article Online
DOI: 10.1039/D5SM00508F

s) shows little change in the network structure, while the later frame projection (60-290 s) shows significant network coarsening.

Figure 5. Contact angle measurement. (A) Schematic of static axisymmetric droplet in equilibrium wrapping around the bundle with radius R_f. The $r_1 = \frac{ds}{dy}$, $r_2 = \frac{y}{\sin(\gamma)}$ are the principal radii of curvature of the liquid interface, R_b – radius of the droplet at the cut-off with angle θ_b between droplet contour and cut-off, γ – the angle between the long axis of the fiber an vector r_2, dx, dy, and ds are very small quantities, and – contact angle with the fiber. (B) Example of droplet contour fit with unduloidal function (Eq. 3) with $R_f = 1.2\ \mu m$, $R_b = 6.5\ \mu m$, $\theta_b = 77\ deg$, and $\theta = 31\ deg$.

View Article Online
DOI: 10.1039/D5SM00508F

Figure 1

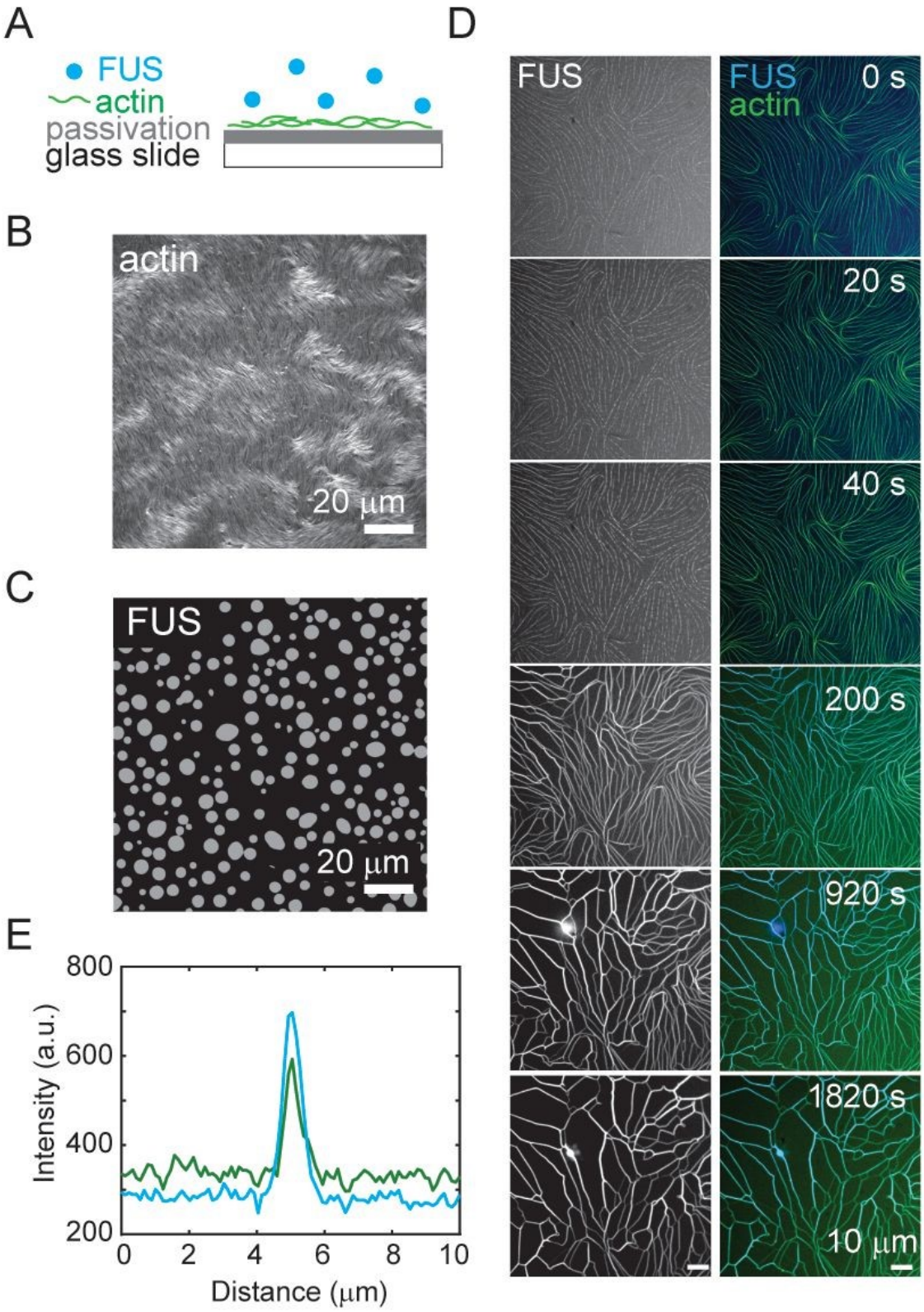

View Article Online
DOI: 10.1039/D5SM00508F

Figure 2

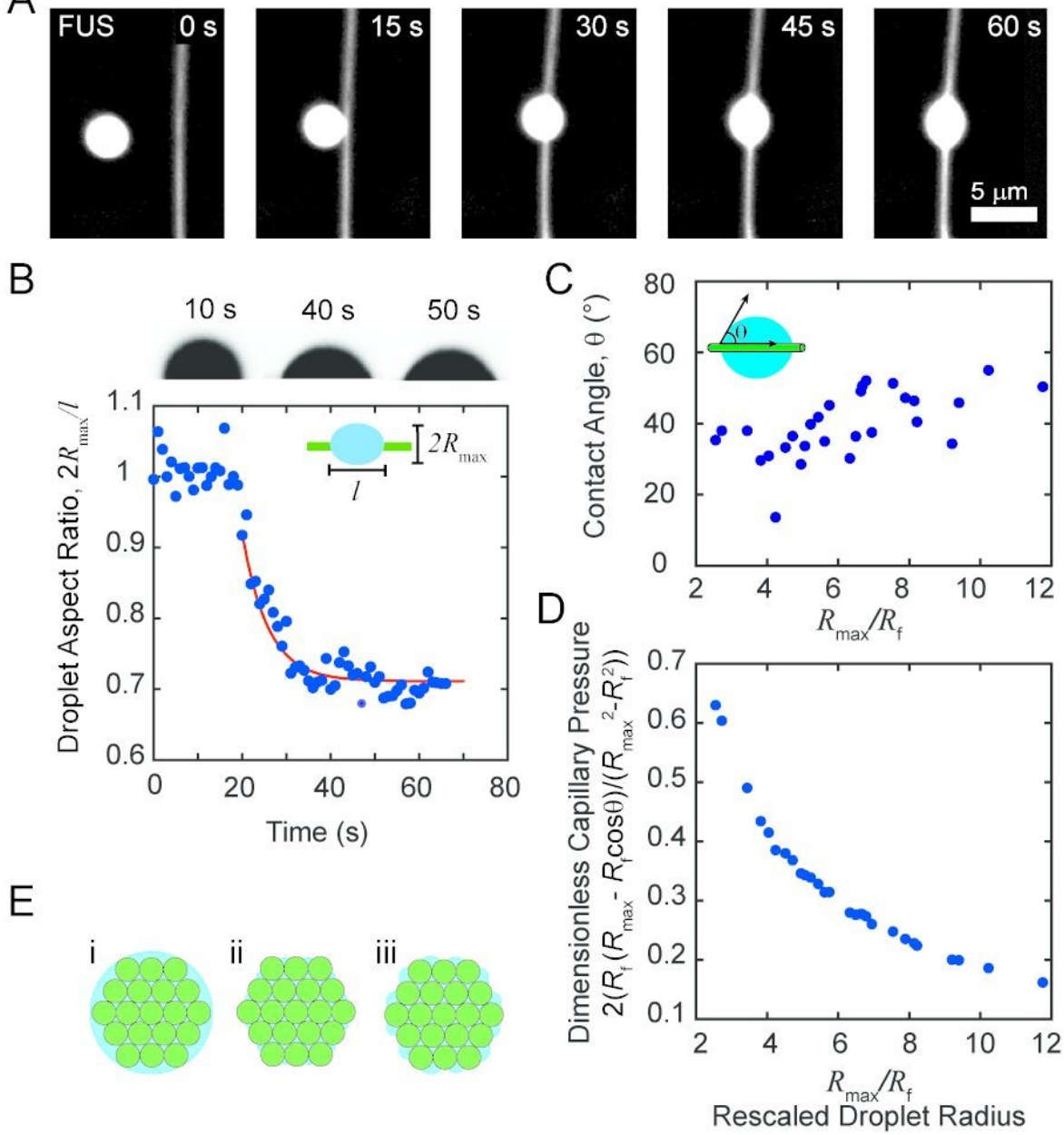

View Article Online
DOI: 10.1039/D5SM00508F

Figure 3

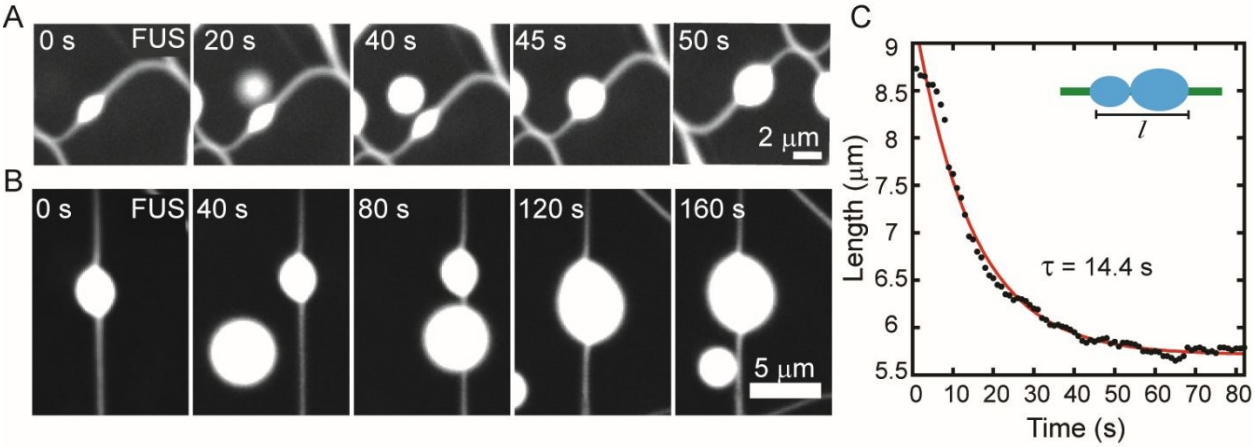

Figure 4

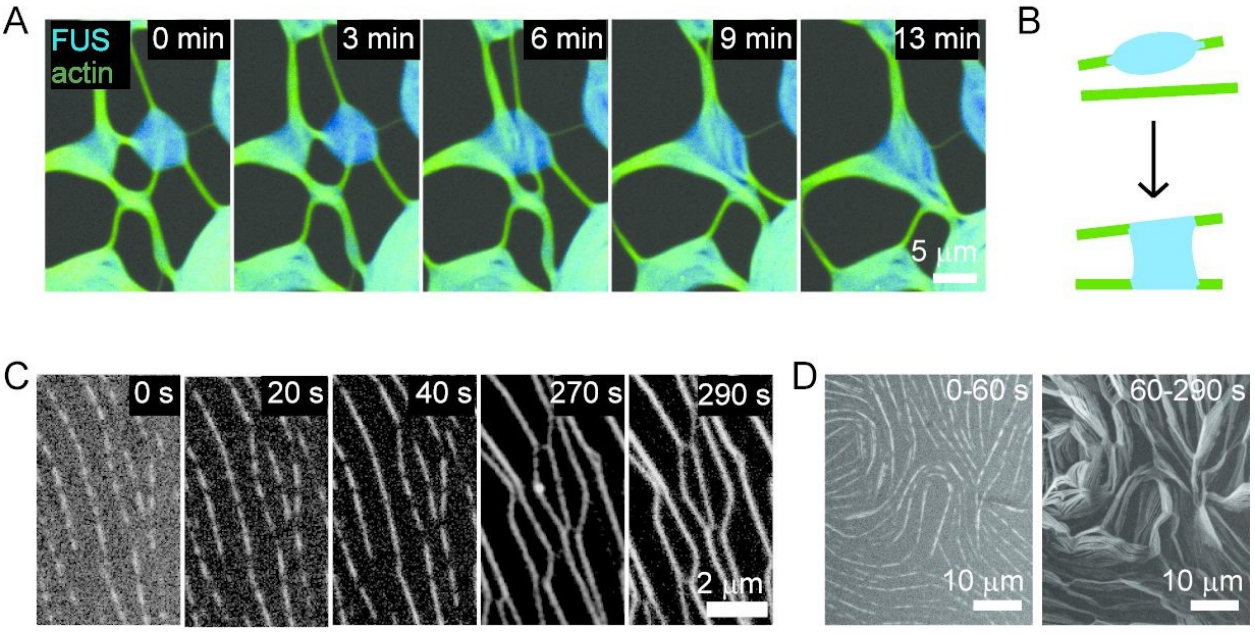

View Article Online
DOI: 10.1039/D5SM00508F

Figure 5

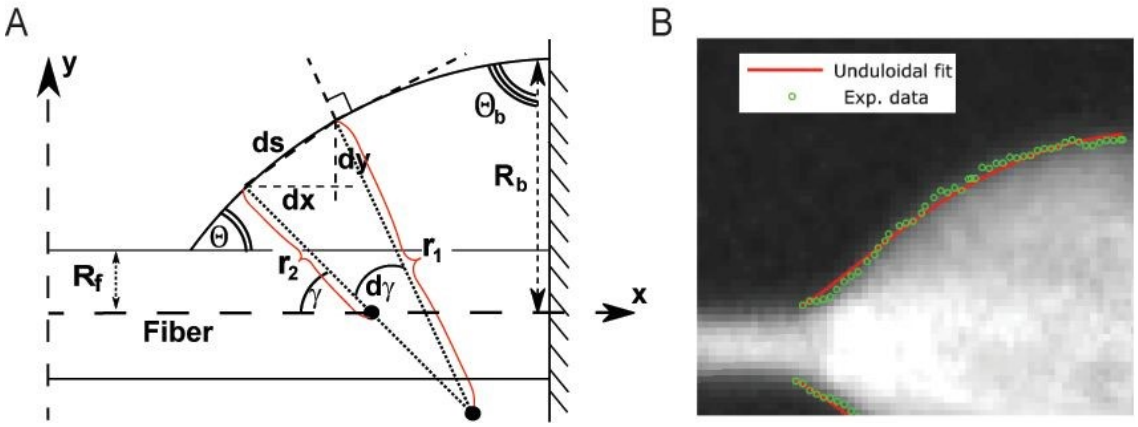

View Article Online
DOI: 10.1039/D5SM00508F

Data Availability Statement

Raw data will be uploaded to Zenodo upon acceptance of this manuscript.